Multifractal structure and intermittent mixing in Rayleigh-Taylor driven fronts

José M. Redondo and Germán Garzon

Dept. Fisica Aplicada, B5 Campus Nord UPC
Universitat Politecnica de Catalunya, Barcelona 08034, Spain

Abstract

Experimental and numerical results on the advance of a mixing or non-mixing front occurring at a density interface due to gravitational acceleration are analyzed considering the fractal structure of the front. The experimental configuration consists on a unstable two layer system held by a removable plate in a box. The initial density difference is characterized by the Atwood number. The evolution of the instability is non dimensionalized by $\tau = (Ag/H)^{1/2}$. As the plate is removed the gravitational acceleration, generates a combination of spikes and bubbles, which reach maximum complexity and local mixing efficiency before the front reaches the end walls. The instability produced is known as Rayleigh-Taylor (RT) instability, and in its simplest forms occurs when a layer of dense fluid is placed on top of a less dense layer in a gravitational field. The instability forms a turbulent front between the two layers developing a cascade of secondary instabilities in a non-homogeneous fashion. A Large Eddy Simulation numerical model using FLUENT is used to predict some of the global features of the experiments, different models on the interaction of the bubble generated buoyancy flux and on the boundary conditions are compared with the experiments. The aspect ratios of the bubble induced convective cells are seen to depend on the boundary and initial conditions applied to the front. The evolution of the Rayleigh-Taylor instability develops into a turbulent mixing front that may be investigated further using the information that the fractal dimensions or Kolmogorov Capacities give as the flow evolves in time. The basic self-similar characteristics of the flow are compared and the evolution of the multi-fractal dimensions of density, velocity and vorticity contours provides indication that most mixing takes place at the sides of the dominant convective blobs. In the context of determining the influence of structure on mixing ability, multifractal and spectral analysis is used to estimate intermittency and determine the regions of the front which contribute most to molecular mixing.

1. Introduction

The stability of an interface between two superposed fluids of different density was studied by Lord Rayleigh and Taylor(1950) for the case when the dense fluid is accelerated towards the less dense fluid, the linear theory can be found in Chandrasekhar (1961). For inviscid fluids, the interface is always unstable, with the growth rate of the unstable modes increasing as their wavelengths decrease. The instability of the short waves can be reduced by dissipative mechanisms such as surface tension or viscosity. For the viscous two-layer case, where the upper layer (density ρ_1) is denser than the lower layer (density ρ_2), the wavelength λ_μ of maximum growth rate is

$$\lambda_m \approx 4\pi\left(\frac{\nu^2(\rho_1+\rho_2)}{g(\rho_1-\rho_2)}\right)^{1/3},$$

where v is the mean kinematic viscosity of the two layers and g is the acceleration of gravity.

The corresponding maximum growth rate is

$$n_m \approx \left(\frac{2g\pi(\rho_1 - \rho_2)}{\lambda_m(\rho_1 + \rho_2)} \right)^{1/2}.$$

While the linear theory for two infinite layers is well established, the development of the instability to finite amplitude is not amenable to analytic treatment. There have been a number of semi-analytical and numerical studies in recent years, but they all involve simplifying assumptions which raise serious doubts about their validity particularly when applications to mixing are sought. An overview of the subject by Sharp(1984) characterized the development of the instability through three stages before breaking up into chaotic turbulent mixing. 1) a perturbation of wavelength λ_μ grows exponentially with growth rate n_μ. 2) when this perturbation reaches a height of approximately ½ λ_μ, the growth rate decreases and larger structures appear. 3) the scale of dominant structures continues to increase and memory of the initial conditions is supposedly lost; viscosity does not affect the latter growth of the large structures. This was observed not to be the case in the experiments of Linden et al.(1995) and in more recent experiments by Dalziel (1994) and Dalziel et al.(1999) with the two dimensional wake and the initial velocity structure affecting the growth of the RT mixing fronts for a long time.

The advance of this front is described in Linden & Redondo (1991), and may be shown to follow $\delta = 2cA\tau^2$ where δ is the width of the growing region of instability, g is the gravitational acceleration and A is the Atwood number defined as $A = \frac{\rho_1 - \rho_2}{\rho_1 + \rho_2}$

This result concerning the independence of the large amplitude structures on the initial conditions has led to consider that the width of the mixing region depends only on ρ_1, ρ_2, g and time, $\tau = t - t_0$. Then dimensional analysis may be used. The parameter c is considered to be a (universal) constant related to the accumulative mixing or entrainment produced by the front, although some dependence with the Atwood number and the initial conditions of the plate removal or random numerical fluctuations is expected.

The value of the parameter c, has been investigated experimentally and its value for experiments at different values of the Atwood number, A, do not show large variations in the case of large A, with an asymptotic limit for the larger *Atwood number* experiments performed. Values of c previously obtained experimentally have been in the range (0.03 – 0.035) (Read and Young 1984) in experiments with three dimensional effects and large density differences between the two fluids, $A \geq 1.5$. Redondo and Linden (1990) measured c for values of A in the range 1×10^{-4} to 5.0×10^{-2} and found values of $c = 0.035 \pm 0.005$. Numerical calculations in two dimensions (Young 1984) have given values of c in the range 0.02 - 0.025. The lesser values (Read 1984) have been explained in terms of two dimensional effects inhibiting the growth of the large scale.

First we describe the experiments and numerical simulations, in section 4 we detail some aspects of the multi fractal analysis performed, comparing in sections 5 and 6 the simulations and experiments. In section 7 we look at the fractal behavior of the different parts of the flow and finally we compare volume fraction, velocity and vorticity descriptions of the RT flow, discussing the results and drawing some conclusions regarding local mixing and front evolution.

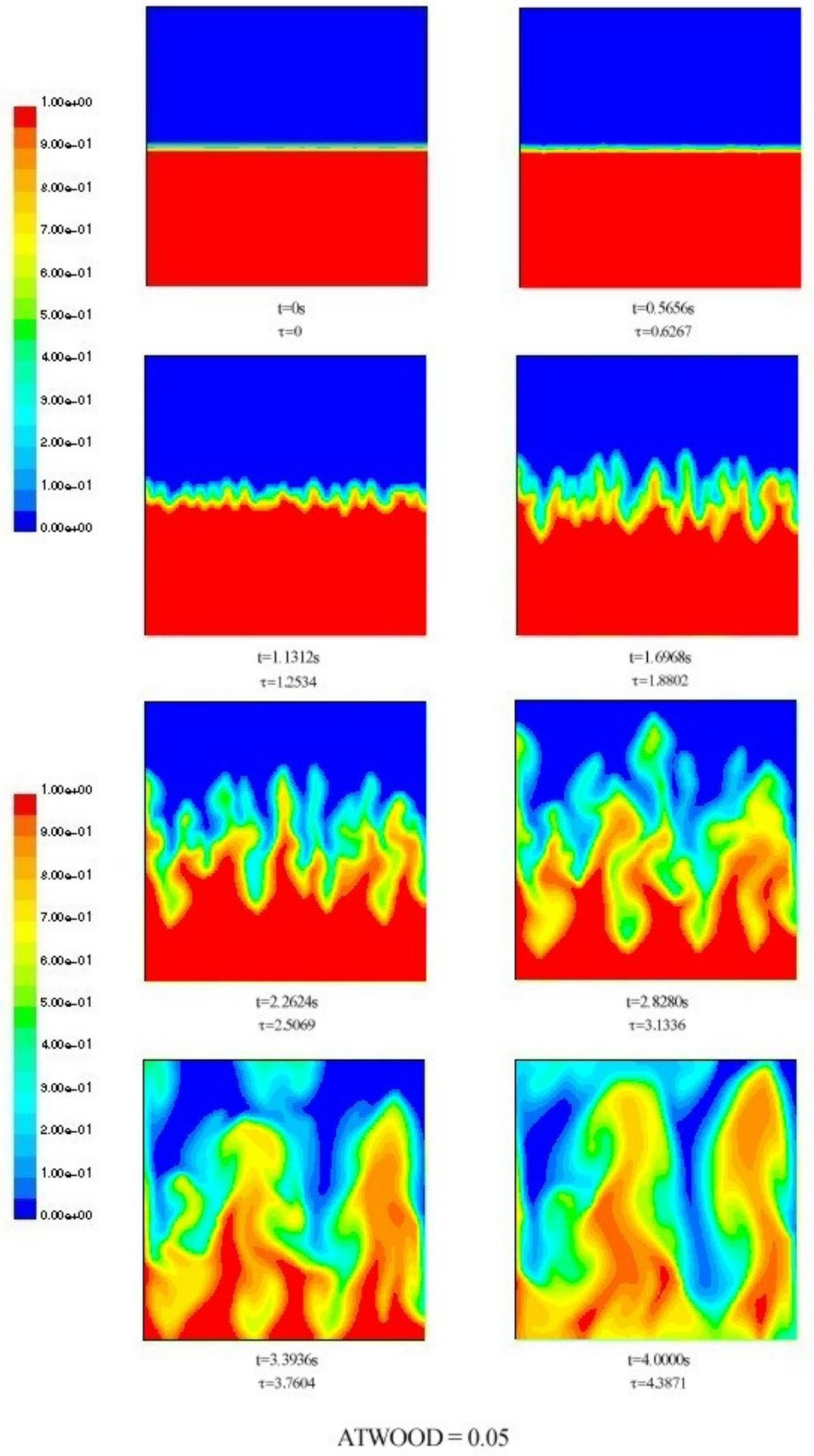

Figure 1. Evolution of the RT turbulent front for A=0.05

2. Description of the RT experiments

The experiments consisted of a release of a dense fluid in a rectangular Perspex tank of height H = 0.50 m, length L = 0.40 m and width W = 0.20 m. The two fluids are initially separated by a removable stainless steal sheet, 1.5 mm thick,
in the centre of the tank. Fresh water is placed in the lower half of the tank and the sheet, sliding in tight fitting grooves, is pushed across and sealed with silicone grease, and finally the dense layer of brine is placed on top. The experiments were initiated by withdrawing the plate horizontally through a seal in the end wall of the tank. A 0.6 W argon laser light passing through an cylindrical lens was used to produce a 2 mm thick sheet of high intensity light. Fluorescein dye was added to one of the layers, and this produces a brilliant green image in the laser light. The leading edge of the advancing front was demarcated by this technique, and images of the small scale structures were obtained in the experiments described in Redondo and Linden (1993). Further analysis allowed for a large range of intensity values to be analysed and not just the Volume fraction concentration contours of 50%.

The fluorescein is only added in very small quantities so that it acts as a passive tracer. Using suitable orientations of the light sheet, side and end elevations and plan views of the flow were obtained. The second method of flow visualization which was used involved the use of a pH indicator to mark the flow where molecular mixing occurs. As discussed in Linden y Redondo (1991), it was necessary to have the Atwood number greater than 0.005 to ensure that the plate did not affect significantly the RT front.

The advance of the mixing front is scaled with a non dimensional time, defined as:

$$T = \sqrt{\left(\frac{Ag}{H}\right)}t\,.$$

As soon as the RT front advances, a series of convective cells are developed from the basic RT instabilities in the centre of the tank, advancing to both upper and lower sides. Figure 1 shows the evolution of these RT cells with Spike or Bubble shapes that are formed.

Dalziel et al. (1999) confirmed constant values of the front growth constant c independently of the density ratio, but these experiments had a very limited Atwood number range. In those experiments, the strong 2D influence of the initial plate wake conditions were highlighted, when comparing the results of a modified “shearless” plate with that used by Linden et al.(1994). The universality of the quadratic time (t^2) behaviour of the growth, nevertheless, was confirmed, suggesting that for a wide range of Atwood numbers the flow develops a wide self similarity.

Different parameters of the convective process, such as the Atwood and Prandtl numbers and the aspect ratio of the bubble laden RT flow have been changed in the numerical simulations in order to investigate the behaviour of the flow. The different sub grid effects needed to model the behaviour of the convective cells in both homogeneous and stratified flows are discussed. The aspect ratios of the initial induced RT cells are seen to depend on the boundary conditions applied to the enclosure and the random initial amplitudes.

3. LES numerical models of the RT front

Large Eddy Simulations solve directly large scale eddies by a Direct simulation of the full Navier-Stokes equation, but model the smaller scales with a numerical scheme, normally

relating local turbulent viscosity to local shear derived from the resolved scales of the numerical calculation. LES considers that momentum, mass, energy and other scalars are mostly transported by the largest eddies; these large eddies are very dependent on the flow conditions and on flow forcing, so their characteristics are dominated by the flow geometry and the boundary conditions. The smaller eddies are more influenced by the numerical mesh and the local shear, which in principle makes them appear more isotropic.

The basic equations of the Large Eddy Simulation are obtained from a filtering of the non stationary Navier-Stokes equations, either in Fourier space (as wave numbers) or in real space configurations. The filtering removes small scale eddies of the grid mesh size used in the calculations. The filtered variables are defined as

$$\bar{\phi} = \int_D \phi(x')G(x,x')dx\,,$$

where $\bar{\phi}$ is the filtered variable, D is the application domain and G is the function that determines the scale of the resolved eddies .

In FLUENT the discretization by means of finite volumes provides in an implicit way the filtering process as.

$$\bar{\phi} = \frac{1}{V}\int_V \phi(x')dx, \quad x' \in V\,,$$

where V is the volume of a computational cell. The filter function used is:

$$G(x,x') = \begin{cases} 1/V & \text{for } x' \in V \\ 0 & \text{for } x' \notin V \end{cases}.$$

As the model of LES used for the simulation of low Atwood number experiments, and it was checked in the experiments that the accelerations are weak, the FLUENT option used for LES was for incompressible flows.

Filtering the Navier Stokes equations for the incompressible case leads to:

$$\frac{\partial \rho}{\partial t} + \frac{\partial \rho \bar{u}_i}{\partial x_i} = 0\,,$$

$$\frac{\partial}{\partial t}(\rho \bar{u}_i) + \frac{\partial}{\partial x_j}(\rho \bar{u}_i \bar{u}_j) = \frac{\partial}{\partial x_j}(\mu \frac{\partial \bar{u}_i}{\partial x_j}) - \frac{\partial \bar{p}}{\partial x_i} - \frac{\partial \tau_{ij}}{\partial x_j}\,,$$

with τ_{ij} being the tensor, associated to the Reynolds stress sub mesh size, defined as:

$$\tau_{ij} \equiv \rho\overline{u_i u_j} - \rho \bar{u}_i \bar{u}_j\,.$$

The practical model at sub grid size used in the simulation was the well known Smagorinsky-Lilly with the value or the constant as Cs=0.1, Cs is termed as Smagorinsky constant. FLUENT allows using either a segregated or a coupled model. In both of these methods, the finite volume system is used and follows the standard procedure as:

Division of the domain in discrete volumes, using the gridding options.

Integration of the individual equations in each control volume to generate a set of algebraic equations for the discrete variables such as: velocity, pressure, temperature, density and other scalars modelled.

Linearization of the discretized equations and solution of the system of linear equations resulting at each time and spatial steps to deliver the set of dependent variables.

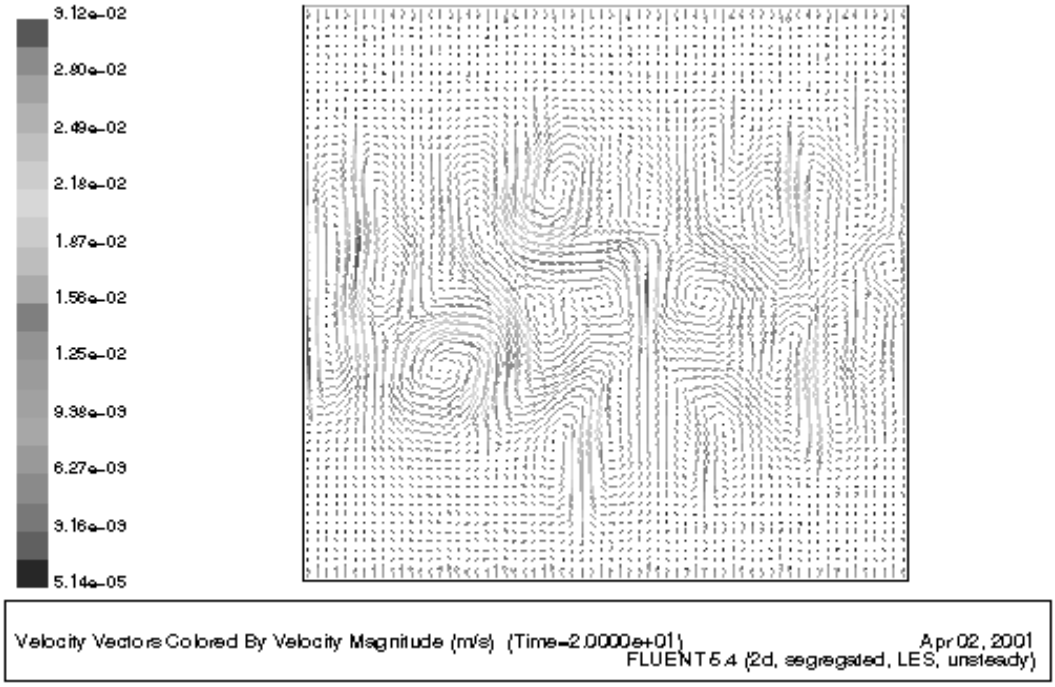

Figure 2. Velocity map of the RT instability at non-dimensional time 2 from FLUENT

To calibrate the numerical model, a series of two dimensional simulations modelling the flow in a 40cm × 40cm. Tank were made with three different mesh sizes, 64×64, 128×128 and 256×256, each with two different Atwood numbers, 1×10^{-4} and 5×10^{-2}.

The method used was the segregated because it is the only one that allows the use of two fluids. The time discretization and time steps used was made in a particular way for each Atwood number, assuring stability, as results were expressed in terms of the non-dimensional number described as:

$$T = \frac{t}{\sqrt{\frac{H}{gA}}},$$

with *H* the tank height, g gravity and A Atwood number.

In figure 3 we compare the results for the same non dimensional times, T=3,2,1, but for two different densities of the numerical mesh.

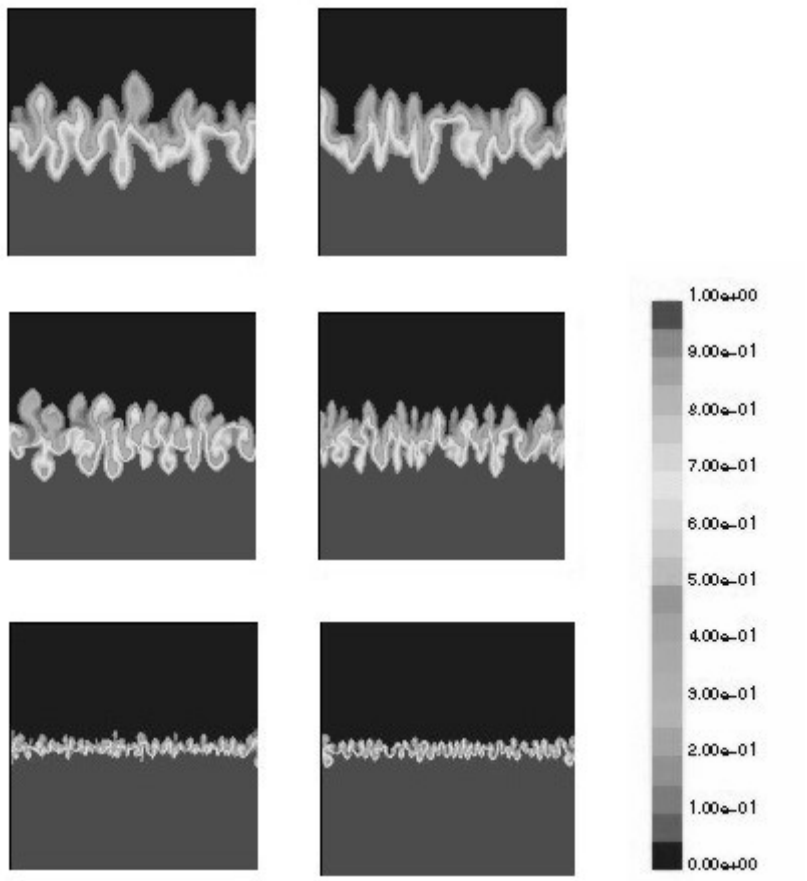

Figure 3. Comparison of the growth of the RT front for meshes 256 (left) and 128 (right) at three times.

We observe that there are no significant deviations of the front growth for different Atwood numbers, but there are differences between the different meshes, especially for the lower resolutions. It was considered that 256 mesh elements provided mesh independence. The evolution of the RT may be seen in more detail in figure 4. The non dimensional times are 1,2,3 and 4 with an Atwood number of 0.0001 for the left column and A=0.05 for the right-hand column.

The larger "blobs" advance master and grow at the expense of the smaller ones. The front shows a constant acceleration. Comparing this behaviour with the growth of 2D and 3D plumes (Turner 1973), we see that the RT instability front growth δ has higher power dependences with both the Buoyancy flux B and with time:

$$\delta = z = cBt^2 \quad \text{for a RT front,}$$
$$z = C_2 B^{1/3} t \quad \text{for a 2D plume,}$$
$$z = C_2 B^{1/4} t^{3/4} \quad \text{for a 3D plume.}$$

4. Comparison of LES RT front models and experiments

In figures 1-4 the sequences of the advance of the mixing front, using the non-dimensional time described above were compared with the experiments. The global aspects of the mixing front are seen to depend strongly on the mesh size used and on the random initial perturbation. Figure 5 presents the evolution of the velocity as the RT front grows. Figure 6 shows a direct comparison of the experiments and LES simulations for the highest resolution mesh. The discrepancy as discussed by Linden et al(1994) is mostly due to the use of a 2D model and to the random initial conditions.

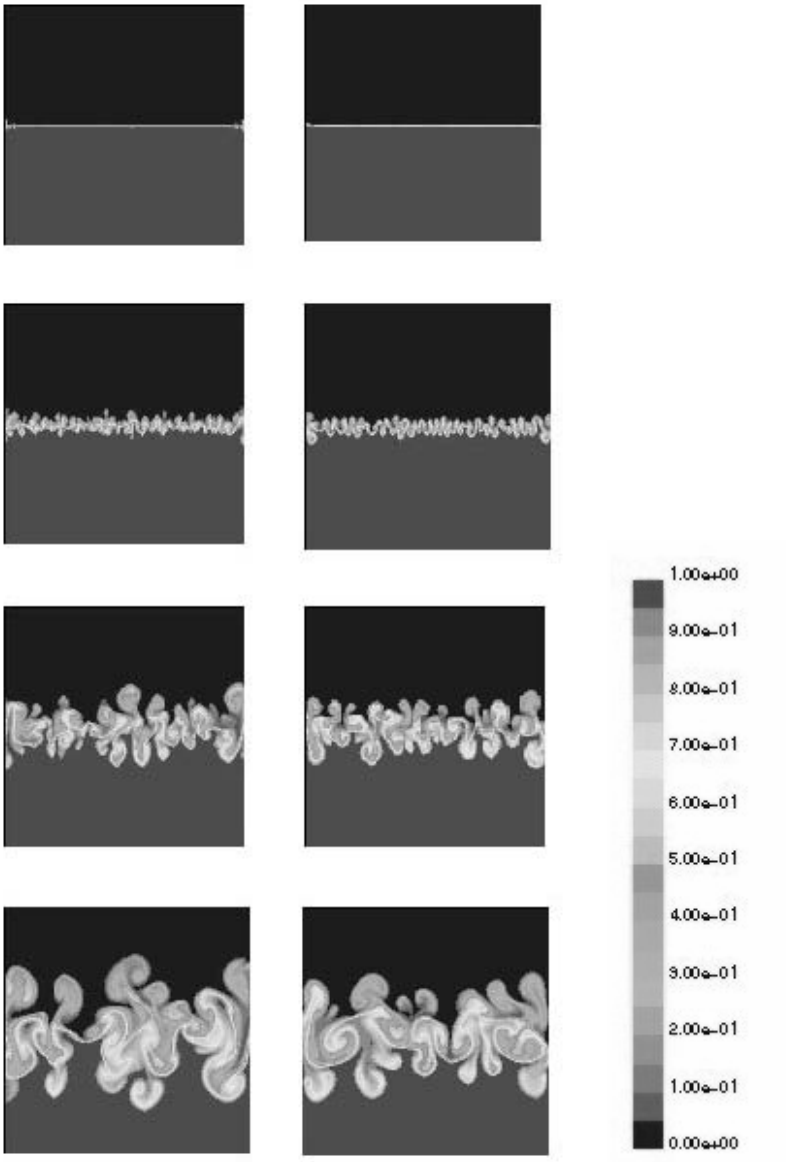

Figure 4. Comparison of the RT fronts for two Atwood numbers 0.001 and 0.05

The evolution of the velocity modulus of the LES Rayleigh-Taylor simulation may be seen in figure 5, These sequences may be also considered as the indication of the Kinetic Energy per unit mass.

The Volume fraction, Energy and Vorticity (or enstrophy) plots of the RT-fronts are very useful in order to compare the degree of self similarity in different regions of the flow and in time.

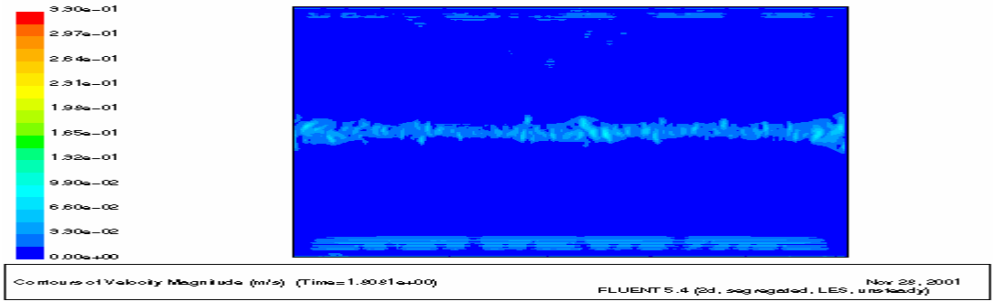

a)

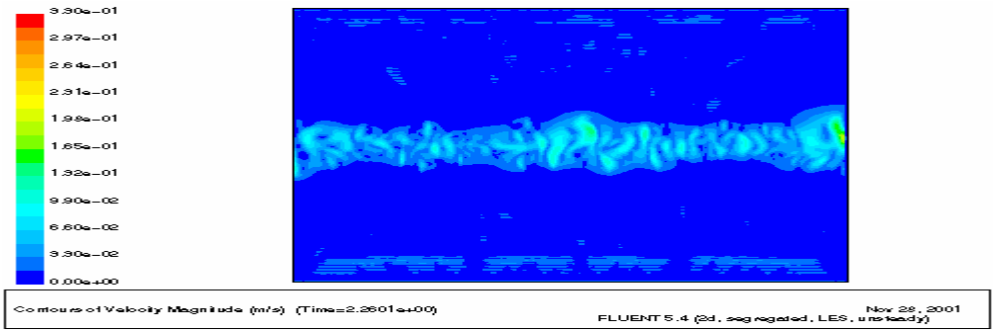

b)

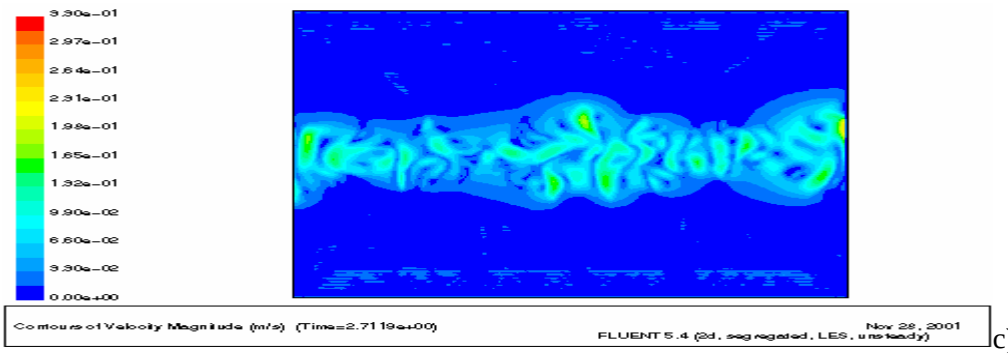

c)

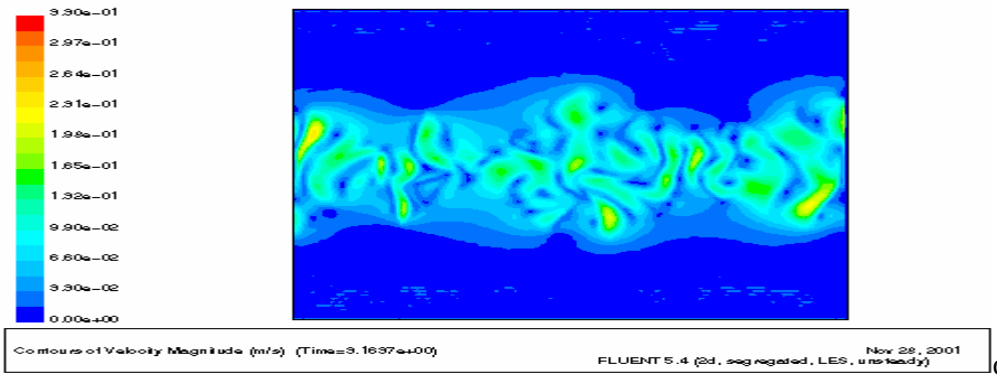

d)

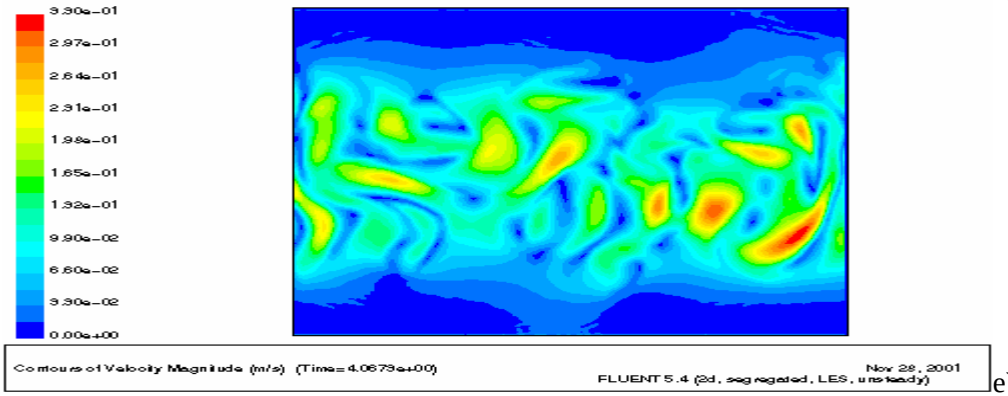

e)

Figure 5: Evolution of the Energy in a RT 2D LES a-e) indicate non-dimensional times 0.5 to 3.5

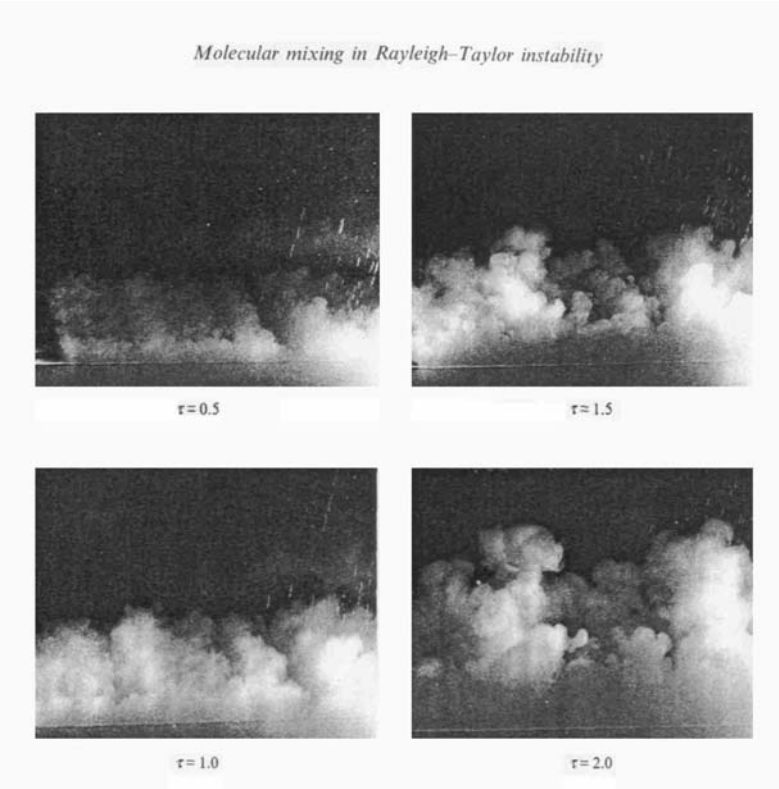

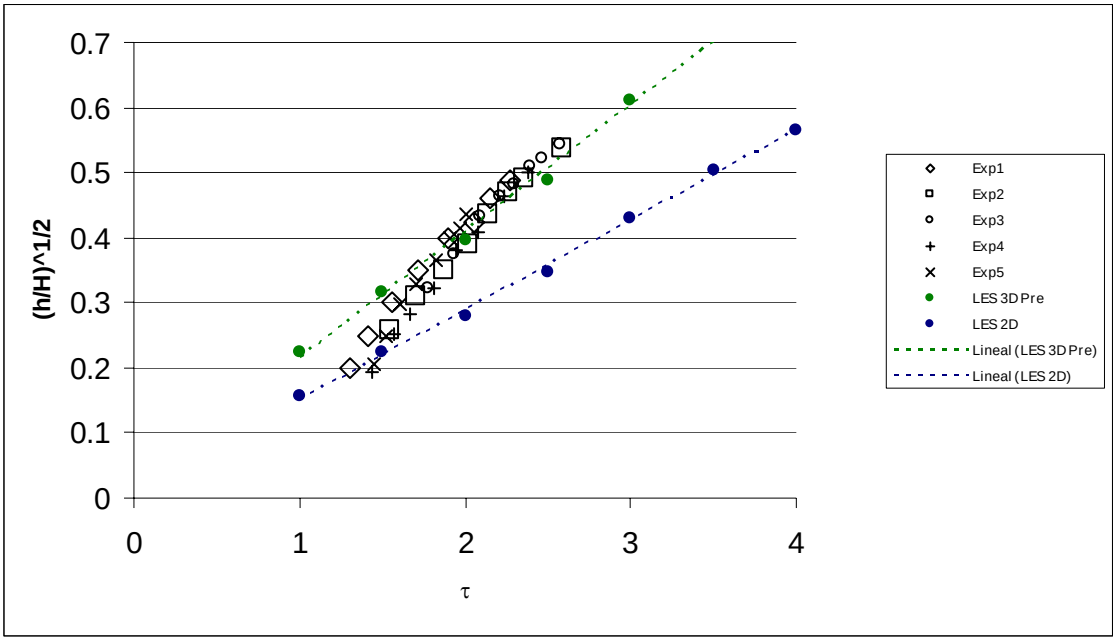

Figure 6: Comparison of the advance of the RT front in Linden et al(1994) with LES numerical simulations, a) 3D images of the experiment, b) Comparison of the front positions in time.

The initial faster growth rate of the experiments is thought to be due to the additional disturbance due to the removal of the plate. It was also clear that the 2D Les models gave a lower growth rate to the 3D LES model used (even being of smaller resolution 64^3).

5. RT front self-similarity

In a similar way as in Linden et al. (1994) where the maximum fractal dimension for the 0.5 volume fraction contours was calculated and compared between the experiments and 3D numerical simulations. We extend her the box counting algorithm to cover a wide range of concentration levels in the numerical simulations as well as applying the multi fractal method to velocity and vorticity images at different times. The box-counting method apply has been described in Redondo(1997) and Villermaux et al(1999), for a theoretical description and further results see the paper in these proceedings Garzon et al.(2004).

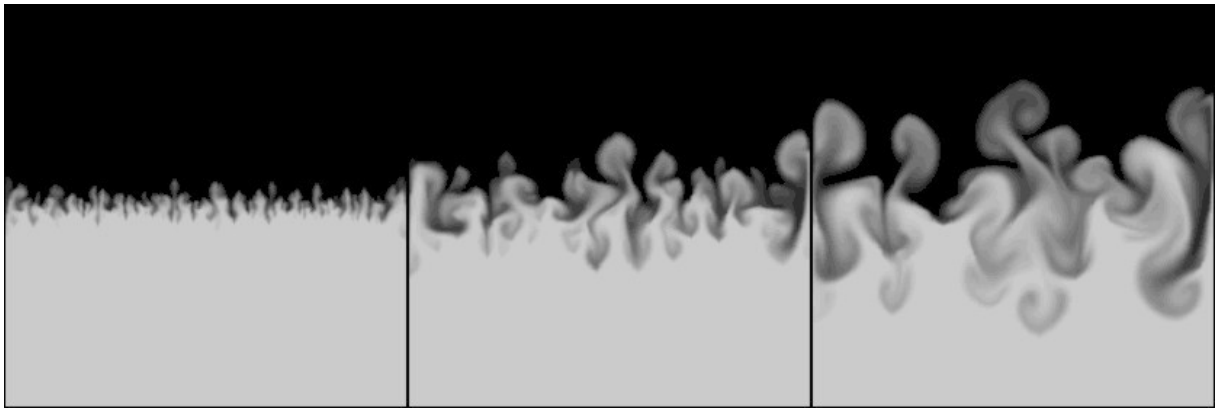

Figure 7 Detailed. Structure of the RT front at times t/T=1,2 and 3.

Analyzing the whole front for velocity and volume fraction at several times gives a value of the fractal dimension for each value of the set analyzed for the different times. From a geometrical point of view this extended analysis provides with much more information on the curdling and self similarity of the interfaces of different values.

The results describe the range of intensity values, where the isoconcentration lines exhibit a fully developed turbulent behavior indicated by a fractal dimension equal or greater that D=1.4 As expected, the turbulent self similar characteristics are shown only in the regions of strong contact between the two fluids.

In figure 8 we present the evolution in time of the set of fractal dimensions for the different values of the Velocity module (right) and the Volume fraction (left). It is the first time such analysis has been applied to the velocity set of values and further interpretation will be necessary, but it is clear that as non-dimensional time advances, the values of the velocity increase and at the same time their convolutions grow giving higher values of the fractal dimension for most values. The slopes of D(v) and the fact that the highest velocity regions in the flow do not exhibit the highest fractal dimensions indicates that it is necessary some additional time for the velocity / Energy cascade to become unstable and to have a higher fractal dimension value. The highest limit of about 1.4 for the planes agrees with previous findings and this value is reached for the velocity at about T=3. This high Fractal dimension value is also reached at T=3-4 for the volume fraction, but only for values between 0.8 and 0.9. The shape of the LES volume fraction values is somewhat smoother than that of the experiments, with values of 1.2-1.3 after T=3.5. The very low values of the initial evolution of the front have to be compensated by a shifting of the virtual origin of the RT instability because of the strong influence of the initial conditions on the early growth rates.

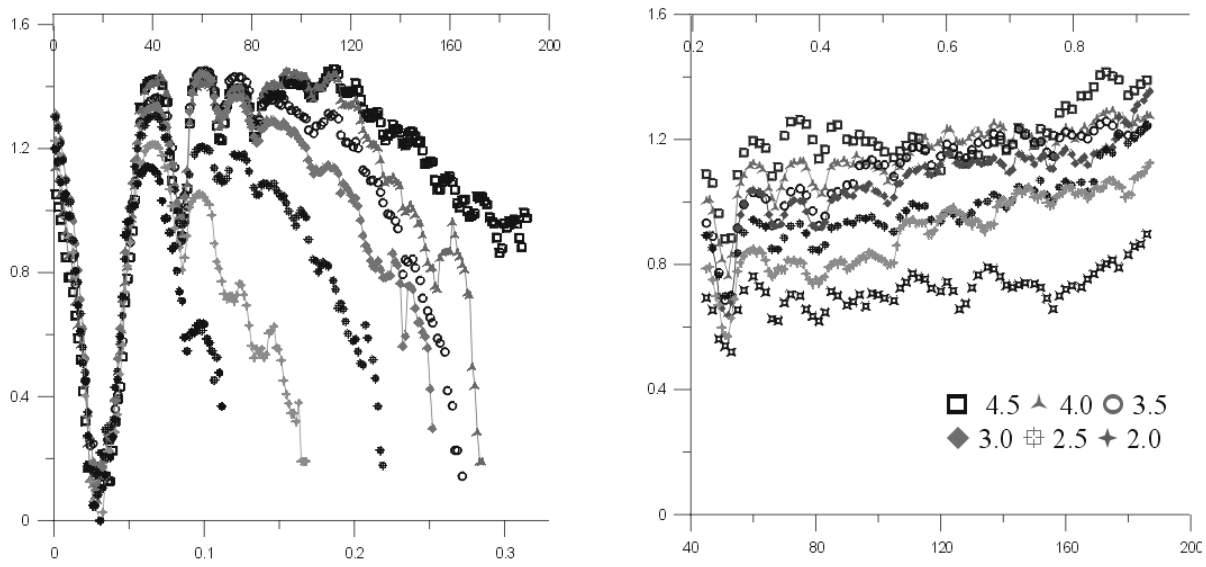

Figure 8. Evolution of the multifractal dimension RT front at non dimensional times t/T=0.5, 1, 1.5, 2, 2.5, 3 and 3.5 (right) Velocity contour analysis, (left) Volume fraction analysis comparable to Linden et al(1994)

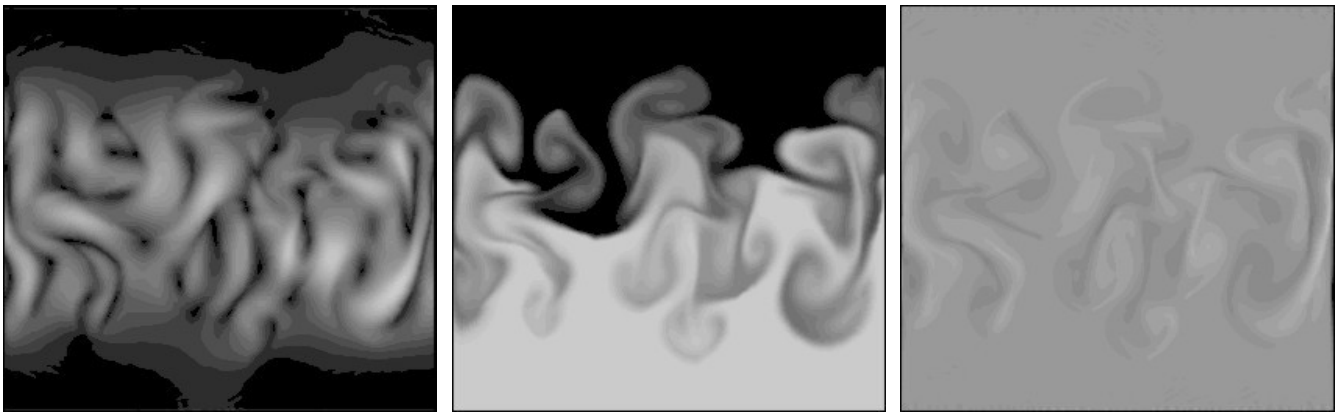

Figure 9. Comparison of Velocity modulus (left), Volume Fraction (center) and Vorticity (right) Contours

The Volume Fraction and vorticity contours are somewhat similar, but their Fractal dimension values are quite different, with smoother (low D(i)) values for vorticity, this behavior is not quite understood.

It is also very interesting to compare different regions of the flow, such as bubble head, bubble sides, spikes and the whole front in order to judge the different levels of fractality for the different concentrations in the selected regions. This procedure may also be applied to the experimental volume fraction images to judge where the LES model reflects correctly the appearance of further secondary instabilities and the turbulent mixing process.

Figure 9 shows the comparison for the same Atwood Number A=0.05 and time T = 3 of the velocity modulus, the volume fraction and the vorticity. The range of values are equalized and normalized for better comparison

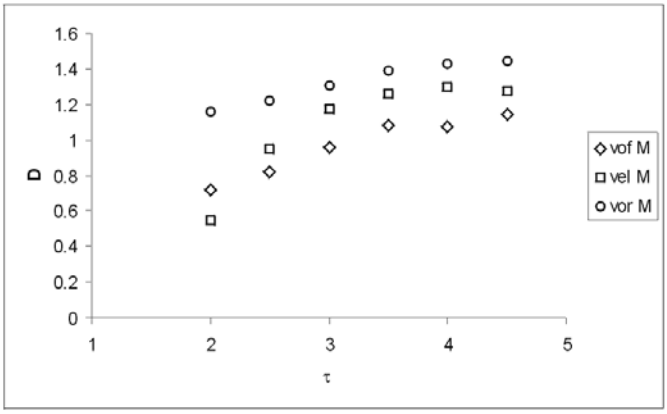

Figure 10. Fractal evolution of volume fraction, velocity and vorticity contours in the development of a RT front

Figure 8, shows the evolution of the multifractal dimension (calculated performing the box-counting algorithm) for each level of velocity modulus (left) and volume fraction (right). Much more relevant information can be extracted from these evolutions than from the maximum value presented by Linden et al.(1994), furthermore it is of great interest to study independently the fractal properties of velocity, volume fraction and vorticity fields as shown in figure 10 only for the intermediate values. Here the evolution of only the intermediate values is presented. Even if the overall vorticity fractal dimension values are smaller than for Volume fraction or Velocity, the range of intermediate values are higher. It may also be seen that the growth of Fractal dimension values for intermediate values of the velocity , as shown in figure 8 grows at a faster rate that either vorticity or volume fraction.

More work is still needed in order to fully interpret the results of the fractal analysis, but it is interesting to compare changes in the fractal dimension with other experimental set ups. Information about the mixing can be extracted from the thickening of the edges due to the phenolphthalein color change in Linden et al. (1995), or in the numerical simulations, and this thickness can be now analyzed with a digitizer system. For lower density runs with phenolphthalein, it was apparent that the vorticity originated by the plate increased mixing at the center of the vortices produced by it. This effect can be avoided using intermediate density differences.

Both in the experiments and in the numerical simulations the fractal evolution that indicates a transition to a turbulent flow is apparent as shown by Linden et al.(1995) by the increase in the maximum fractal dimension of the interface center (50/50 mixing ratio) between Dm = 1 and 1.4. The Spectra and fractal aspects of the numerical simulations are compared with the experiments, for example in figure 11 a scatter-plot of the multi-fractal dimension at two times of the different volume fractions of the front indicates its non-uniform curdling

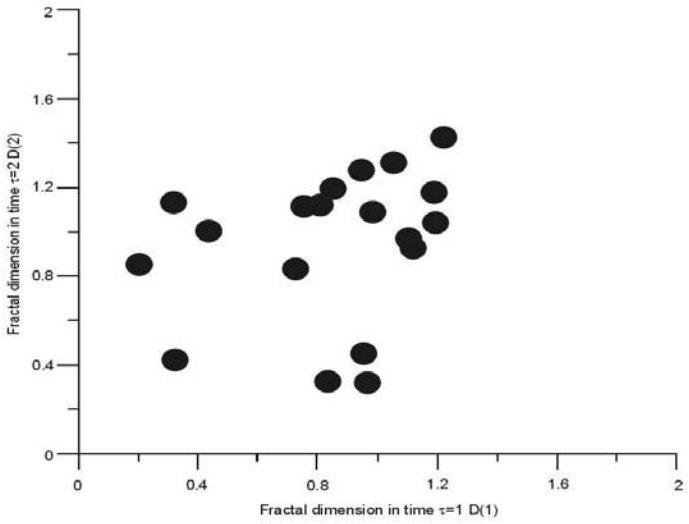

Figure 11. Scatter-Plot of dimension D at two different non dimensional times

Thee relation between fractal analysis and spectral analysis can be very useful to determine the evolution of scales. Presently the emerging picture of the mixing process is as follows. Initially a pure RT instability with lengthscale appears, together with the disturbances from the plate. The growth and merging of disturbances favors the appearance of several distinct blobs, bubbles or protuberances which produce shear instabilities on their sides. These sometimes develop further secondary shear instabilities. After 2/3 of the tank three dimensional effects have broadened the spectrum of lengthscales widely enough as to have a fractal structure in the visual range with dimensions ranging between 2.15 and 2.30 (assuming that $D_2=D_1 + 1$). Some differences may be detected in the maximum fractal dimension evolution in time for experiments with different Schmidt or Prandtl numbers as described in Redondo (1996).

There are several features associated to the stratification and the fractal dimension is one of them. This was first introduced by Redondo (1990), whose experiments on grid stirred stratified turbulence show how a non stratified fluid exhibits higher fractal dimensions than in the case of a stable system dominated by stratification. In the first situation mixing and local entrainment are stronger and the vertical scales of motion are not suppressed. The range of scales and the fractal dimension decreases as the fluid looses its geometrical self-similarity when the local Richardson number, Ri, increases.

In the interval comprised between $10 \leq Ri \leq 100$ we can consider a description of the Fractal dimension in terms of *Ri* as:

$$D = kRi^{-1/2}$$

Where *D* is the fractional part of the fractal dimension in a two-dimensional space and k an experimental constant ($k = 1.4 \pm 0.15$). For the RT instabilities, it may be argued that *Ri* is negative.

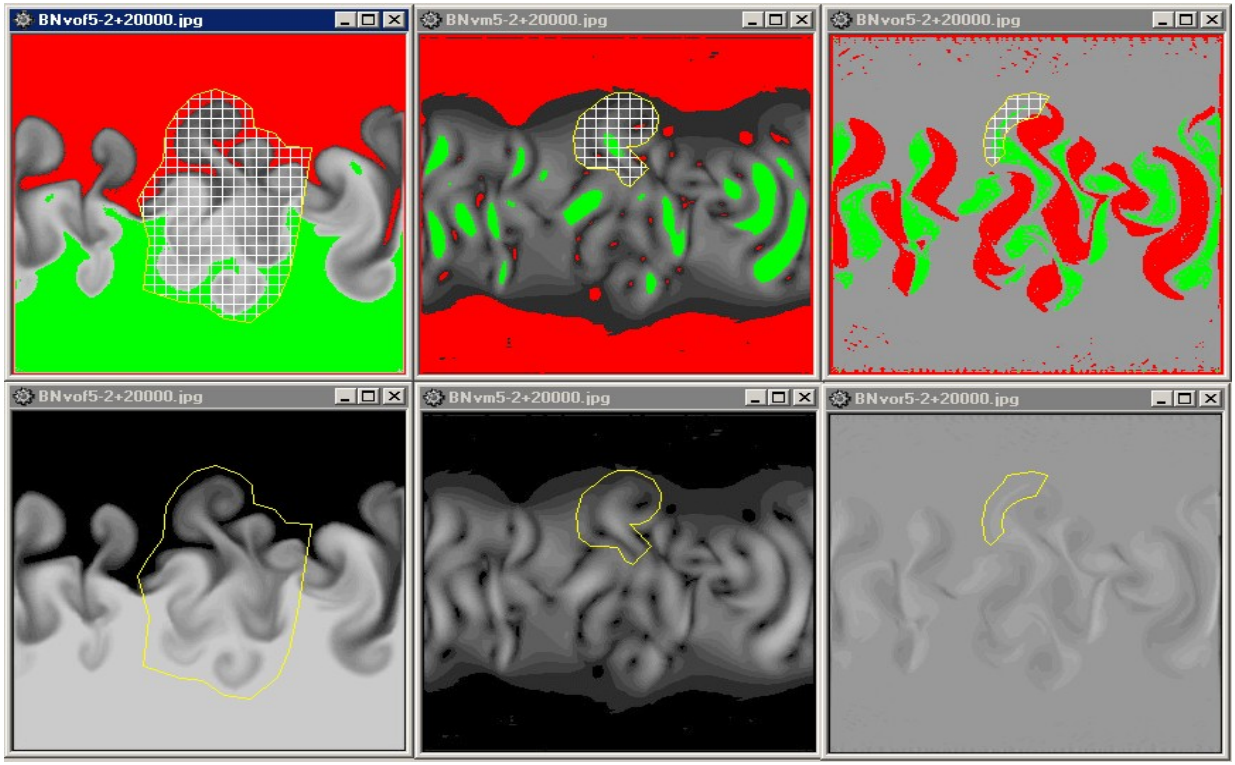

Figure 12. Different regions of analysis used to compare the multi Fractal dimension values. (left) Total Front structure. (centre) RT single blob,. (right) Head of RT instability , Green and Red limit the intensity value range.

For the different regions shown in figure 12, the evolution in time of the Maximum fractal dimension values is presented in figure 13. It can be seen that the heads of the bubbles are effectively not fractal, but show smaller values than for an Euclidean dimension of D=1. Indicating that the values show as sets of disconnected points in the Front of the RT Mushroom shaped RT instabilities. The limit of 1.2 at T=4.5 for the whole front and for the sides of the RT blobs or Mushrooms is somewhat smaller that the experimental values but the difference between the smoother head fronts and sides are a clear indication that most mixing takes place through the sides of the RT blobs.

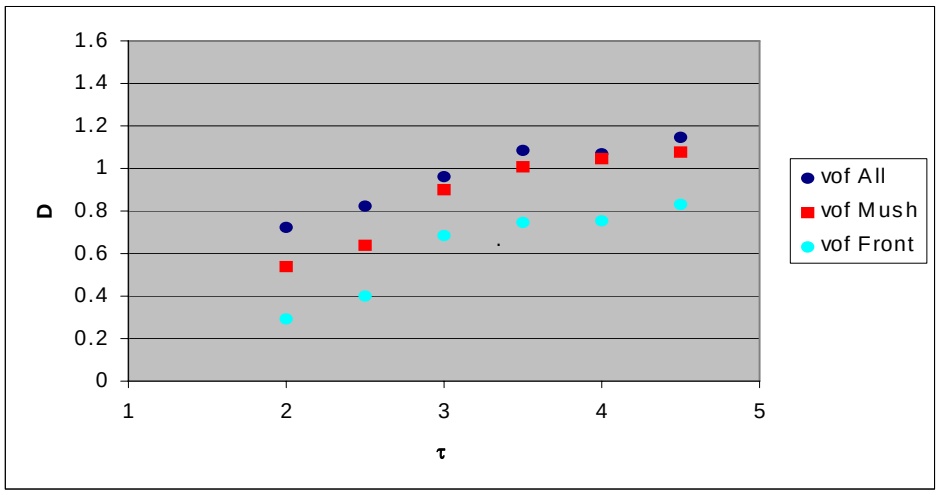

Figure 13. Evolution of the Average Fractal Dimensions for the whole RT front (All), the RT Mushroom shaped blobs (Mush) and the Head fronts (Front)

6. Comparative Analysis of Richtmeyer-Meshkov Fronts

A number of numerical experiments on R-M front mixing forced at a range of intial conditions, which included different amplitudes and wave numbers (as reported by Rozanov et al. 2003) was investigated using the multi fractal approach described above, see figure 14 for an example.

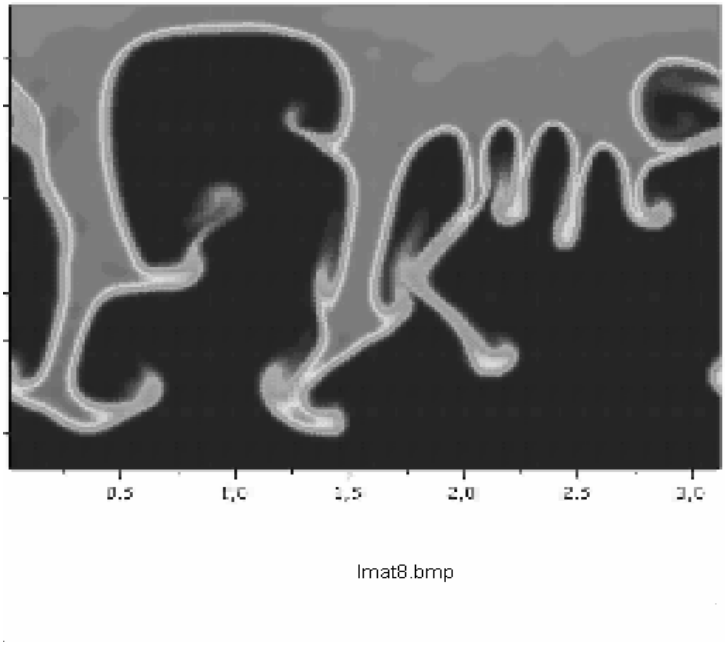

Figure 14: development of a R-M front (FIAN LEBEDEV simulation)

The evaluation of spike and bubble growth showed a much larger asymmetry than for the R-T fronts, due to the lower resolution at the spike heads and to the larger volume fraction gradients

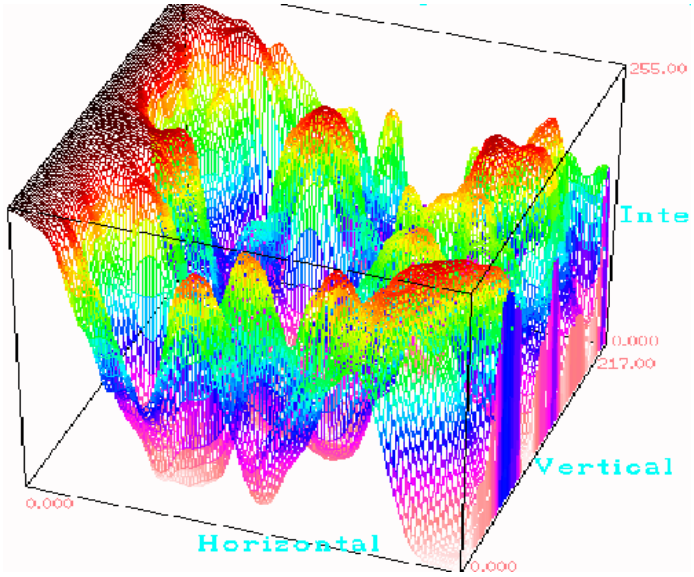

Figure 15. Structure of the heads of the RM instability, the fractal dimension D for different levels of intensity, here indicated as heights/colours for small non dimensional times.

The fractal dimension, given by the slope of the plots such as those in figure 16, which were calculated near the maximum values for plots such as those of figure 14 for the volume fraction. Both Programs DigImage and ImaCalc were used to calculate multifractal dimensions.

The global mass and heat flow may be evaluated if the two different miscible layers have different solute concentrations and different temperatures. In the model as well as in the experiments the density difference may be caused by both salt and heat. The Prandtl number for water is Pr=6.8 and the Schmidt number for brine is Sc=812 at 22C. The Sherwood number defined as Sh=$h_m L/D$ and the Nusselt Number Nu = hL/k_f were calculated as averages over the center region of the interfacial region leaving D/4 to the sides of the numerical domain (or experimental box sides) to avoid lateral influences from the walls

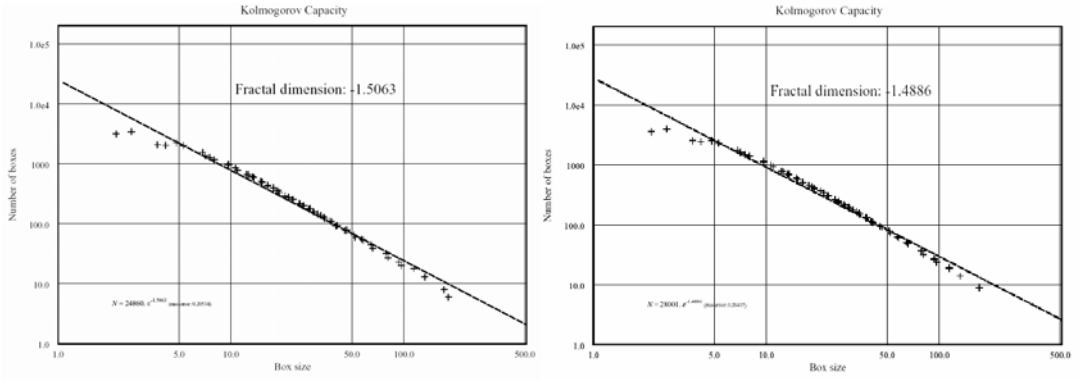

Figure 16. Fractal dimension of the RT instability, the maximum fractal dimension D is given by the Slope

A convoluted line, which is embedded in a plane (that is why it is usually referred to as D_2, or fractal dimension within an Euclidean plane of dimension 2). If it is a single Euclidean line, its (non-fractal) dimension will be one. If it fills the plane its dimension will be two.The box-counting algorithm divides the embedding Euclidean plane in smaller and smaller boxes (*e.g.*, by dividing the initial length L_0 by n, which is the recurrence level of the iteration). For each box of size L_0/n it is then decided if the convoluted line, which is analysed, is intersecting that box. The number $N(i)$ is the number of boxes which were intersected by the convoluted line (at intensity level i). For example different regions of the flow have different maximum fractal dimensions *D(i)*as shown in section 4 and in Garzon et al (2004):

Table 1 *Comparison between Maximum fractal dimension D(i) values for volume fraction contours for RT and RM instability driven fronts*

Atwood Number	Rayleigh-Taylor		Richtmyer-Meshkov	
	t/T=2	t/T=3	t/T=2	t/T=3
$5x10^{-2}$	1.12	1.34	1.30	1.40
10^{-2}	1.20	1.36	1.27	1.46

7. Local Intermittency and fractality

The multi fractal technique performed on the Rayleigh Taylor and Richtmyer Meshkov fronts so far allows discrimination between the strong mixing areas and those weaker mixing regions that produce large smooth interfaces. We have analysed the Fractal and Multi-scale instabilities leading to mixing due to RT and RM instabilities. Using also wavelet and Neural techniques coupled with the multi fractal measurements as described in Garzon et al. (1994) aid the description of the self similar structure of the mixing fronts. An important consideration apparent in the evaluation of the intermittency and the multi fractal dimensions (for different levels of the marker) is that velocity, vorticity and volume-fraction or scalar concentration exhibit different scaling laws.

This has lead to new parametrization techniques for example using Smagorinsky type of eddy diffusivity closures that depend on the active range of scales (i.e. Fractal dimension). Still further comparisons need to be made between numerical simulations with different initial conditions. The regions of higher local fractal dimension increase, both in number and with higher values as time evolves for both the RT and the RM experiments until a non-dimensional time of 3-4 after that time the decrease of the RM front is faster than that of the RT. On the other hand the RM fronts achieve faster a self similar fully turbulent level that corresponds to a fractal dimension of 1.4-1.5 for a wide range of velocities and volume fractions. Both the Sherwood and Nusselt numbers seem also to depend on the maximum fractal dimensions.

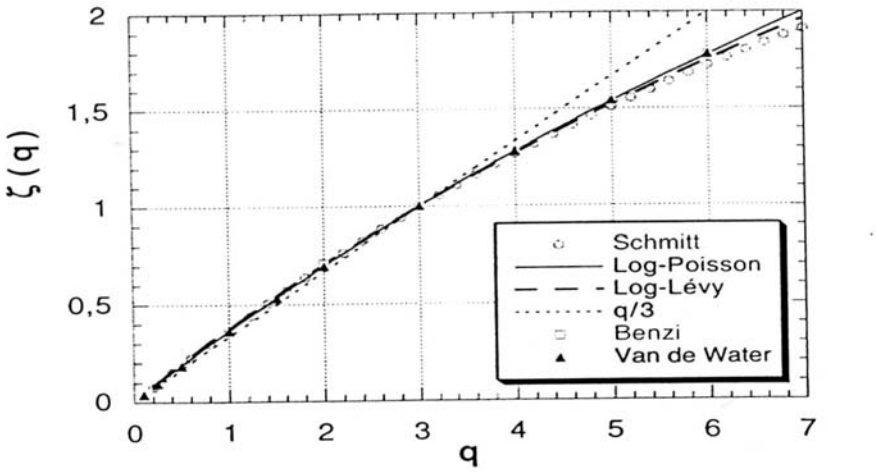

Figure 17. Scaling exponent dependence with order q

In recent years, new interest has emerged concerning the scaling properties of turbulence flows. They are reflected in the scale invariance of Navier-Stokes equations, both in two dimensions (2D) and three dimensions (3D).The statical behaviour of two-dimensional and trhee-dimensional fully developed turbulence at large and small sacles has been intensively investigated in the last years. A common way to board this problem is through the velocity structure functions. Usually studies the scaling properties of moments of velocity differences at the scale r:

$$S^q(\delta u) = < (u(x) - u(x+r))^q > = C(\varepsilon) \quad r^{\xi_q}$$

,

where $< >$ stands for ensemble average and u is the velocity compenent parallel (or perpendicular) to r. At high Reynold number, Re, the scaling exponents satisfy the relation:

For L > r >>η, where the L is the integral scale,η is the dissipative (Kolmogorov) scale, with the dissipation calculated as $\epsilon = {}^{15}\nu \left\langle \left| \frac{dv}{dx} \right|^2 \right\rangle$ as the mean energy dissipation rate, ν is the fluid kinematic viscosity and V is the mean velocity of the flow.
In general, one can definie the scaling exponents of the structure functions in the inertial range where $L > r >> \eta$, by Kolmogorov's 1941 theory (K41), that predicts that the statistical properties of the velocity depend only on ϵ and r, it then follows by dimensional analysis that the scaling exponents $\xi_q = q/3$, but in many experimental and numerical simulation at very high Re, has show that Kolmogorov scaling is violated and that the scaling exponents are nonlinear function of q as shown in figure 17. From a practical point of view, the inertial range is defined by the range of scales where the third-order structure function follows the K41 law, It is precisely in this region where a fractal behavior or either the velocity or of any advected scalar should be detected.

The larger the Reynolds number, the broader the inertial range but for the low to moderate Reynolds numbers accessible to direct numerical resolution, this range is often very narrow. In these cases such as a non-homogeneous RT flow we may apply The Extended Self-Similarity ESS as a property of velocity structure functions in turbulence. It states that when the moments are plotted against another, then the scaling is much more pronounced. In the other words, the ratio of two scaling exponents stays constant for a wider range of scales than each of them does when taken separately. The ESS scaling comprises not only the inertial range, but also reaches as far down as few Kolmogorov scales, so we may compute the scaling exponents with much higher accuracy even at relatively moderate Reynolds numbers. Another important feature of ESS is that it provides information in terms of the relative scaling exponents, which are more universal in that they remain valid also in a 2D case. But this kind of scaling universality, observed in different flows, often disappears if the systems is influenced by the presence of a strong mean shear, In terms of the velocities, the scaling exponents of up to 6^{th} order are calculated, details on the procedure is shown for different experiments in Mahjoub et al.(1989) and Mahjoub(2000).

In this case, for the Rayleigh Taylor flows under non-homogeneous conditions, we are able to obtain a better quantification of the intermittency using ESS in a 2D section of the flow such as that in figure 12. The relationship between intermittency, the fractal dimension at the sides and centers of the RT blobs is obtained using the sixth order structure function and the β-model using:

$$\mu = 2 - \zeta_6 \qquad \zeta_6 = \frac{q}{3} + (3 - D)\left(1 - \frac{q}{3}\right)$$

where q is the order of the structure function , in this case $q=6$, in a similar way, the fourth order structure function may also be used in a simpler way ($\mu=2/3- \varsigma_4$) as described by Frish(1992).

8. Discussion and Conclusions

It is interesting to relate D to the frequency spectrum or to the spatial spectra obtained from the Fourier transform of the time or spatial correlation functions, usual in studies of turbulence. The reason is that from such frequency spectrum the corresponding fractal dimension may be derived, if the tracer scalar is passively advected by a turbulent flow. Then the fractal dimension might be related to the energy of the turbulence with a certain spatial or temporal dependence, then the frequency spectrum exponent, provided an inertial subrange

exists, is a function of the box-counting fractal dimension as demonstrated by Redondo (1990).

However, as a result of Landau's observation, Kolmogorov modified his K41 theory, in 1962, in order to incorporate the non universality of his constant: the turbulent energy dissipation ε should also depend on the length scale. So in K62, Kolmogorov introduced the notion of intermittency, and he would transpose the universality character of his previous constant to the universality of his new parameter, the intermittence, μ. We know that μ is not universal, as it varies from approximately 0.2 to 0.7, according to different experiments. The new energy spectra, *E(k)*, has a correction term in its power of *k*: -5/3 becomes –5/3–μ/9, thus, the global form of the spectra is $E(k) \sim k^{-\beta}$. An interesting approach, relating the Fractal dimension, the intermittency and the spectral exponent is to find relationships that may be used to parameterise the sub-grid turbulence in terms of generalized diffusivities that take into account the topology and the self-similarity of the Mixing RT and RM flows. As an example, a relationship between the diffusivity, the exponent *β*, the intermittency μ, and *D(i)*, may be found for the volume fraction or the concentration, at the same time other locally measured parameters such as the enstrophy or the gradient alignment as well as their multi-fractal structures may turn out to be physically relevant indicators of the local turbulence and the mixing.

Several methods of deriving local eddy diffusivity should give more realistic estimates of the spatial/temporal non-homogeneities (and intermittencies in the Kolmogorov 62 sense obtained as spatial correlations of the turbulent dissipation, or from structure functions) and these values may be used to parameterise turbulence at a variety of scales. The method involving the multi-fractal dimension measurements is much more elaborated and seems to have a better theoretical justification in the sense that it is possible that different concentrations showing different fractal dimensions may be due to different levels of intermittency (and thus different spectra, which are not necessarily inertial nor in equilibrium.

Using fractal geometry as well, we can establish now a theoretical baseline pattern for the turbulence behaviour that is reflected in the different descriptors (volume fraction, velocity and vorticity we can thus obtain a certain classification relating D_3 and the sum (integral) of the different fractal dimensions D_2 for different levels of scalar (volume fraction intensity or temperature). Vorticity evolution is more smooth and quite different than that of volume fraction or density and these seem also different for the RT and RM instability driven mixing fronts.

ACKNOWLEDGMENTS

Support from European Union through ISTC-1481 and INTAS- projects, and from MCT-FTN2001-2220 and DURSI XT2000-0052 local projects are acknowledged

References

Burrows K.D., Smeeton S.V. & Youngs D.L. (1984) "Experimental investigation of turbulent mixing by Rayleigh-Taylor instability II" AWRE report O 22/84

Taylor G.I.(1950) Instability of superimposed fluids, Proc. Royal Soc

Youngs D.L.(1984) "Numerical simulation of turbulent mixing by Rayleigh-Taylor Instability , Physica D,12.

D.L. Youngs. (1997) Proc of the Sixth International Workshop on the Physics of Compressible Turbulent Mixing, France, Marseille, p.534-538.

D.L.Youngs (1989) Modeling Turbulent Mixing by Rayleigh-Taylor Instability, Physica D, 1989, 37, p 270-287

Chandrasekhar S.(1961), " Hydrodynamic and Hydromagnetic Stability" (Oxford Univ. Press,Oxford)

Cole R.L. & Tankin (1973) "Experimental study of Taylor instability". Phys. Fluids 16 (11), 1810-1820.

Linden P.F. & Redondo J.M. (1991) "Molecular mixing in Rayleigh-Taylor instability. Part 1. Global mixing". Phys. Fluids. 5 (A), 1267-1274.

Linden P.F., Redondo J.M. and Youngs D. (1994) "Molecular mixing in Rayleigh-Taylor Instability" Jour. Fluid Mech. 265, 97-124.

Linden, P.F., Redondo, J.M. & Caulfield, C.P. (1988): Molecular Mixing in Rayleigh - Taylor Instability; in Proceedings of 2nd International Workshop on the Physics of Compressible Turbulent Mixing, p. 95 - 112.

Redondo, J.M. (1997): Fractal Characteristics of Reactive Fronts and Shock Tube Mixing Layers in Proceedings of 6th International Workshop on the Physics of Compressible Turbulent Mixing, Ed. G. Jourdan & L. Houas; 422 - 427.

Villermaux, E. and Innocenti, C., "On the Geometry of Turbulent Mixing". Fluid Mech. (1999), vol. 393, pp. 123-147.

D.H.Sharp,(1984) "An overview of Rayleigh-Taylor Instability", Physica 12D,3

Redondo J.M. and Linden P.F.(1990) "Mixing produced by Rayleigh-Taylor Instabilities" Proceedings of Waves and Turbulence in stably stratified flows, IMA conference. Leeds 18 Dec 1989. Ed. S.D. Mobbs.

Redondo J.M. (1996) "Vertical microstructure and mixing in stratified flows" Advances in Turbulence VI. Eds. S. Gavrilakis et al. 605-608.

Kolmogorov, A. N. (1941). The Local structure of turbulence in incompressible viscous fluid at very large Reynolds numbers. C. R. Acad. Sci URSS **30**:301.

Ben-Mahjoub O., Babiano A. y Redondo J.M. (1998) Velocity structure and Extended Self Similarity in non-homogeneous Turbulent Jets and Wakes. Journal of Flow Turbulence and Combustion. 59 , 299-313.

Mahjoub O.B. (2000) Non-local dynamics and intermittency in non-homogenous flows. Doctoral thesis, Universitat Politecnica de Catalunya, Barcelona

Fung, J. C. H., Hunt, J. C. R., Malik, N.A., and Perkins, R. J. (1992). Kinematic simulation of homogeneous turbulence by unsteady random Fourier modes. J. Fluid Mech. **236**:281.

Richardson, L. F.(1929). A search for the law of atmospheric diffusion. Beitr. Phys. frei. Atmos. **15**: 24.

Zouari, N. y Babiano, A. (1994). Derivation of the relative law in the inverse energy cascade of two-dimensional turbulence. Physica D **76**:318.